

SE+BSF4DM - A micrOMEGAs package for Sommerfeld Effect and Bound State Formation in colored Dark Sectors

Mathias Becker ^{1,2,*} Emanuele Copello ^{3,4,†} and Martin Napetschnig ^{3,4,‡}


¹*Dipartimento di Fisica e Astronomia, Università degli Studi di Padova, Via Marzolo 8, 35131 Padova, Italy*

²*INFN, Sezione di Padova, Via Marzolo 8, 35131 Padova, Italy*

³*PRISMA⁺ Cluster of Excellence & Mainz Institute for Theoretical Physics,
Johannes Gutenberg-Universität Mainz, 55099 Mainz, Germany*

⁴*Technical University of Munich, TUM School of Natural Sciences,
Physics Department T70, 85748 Garching, Germany*

(Dated: December 3, 2025)

We present  **SE+BSF4DM**, a novel add-on package for micrOMEGAs that includes the Sommerfeld effect and bound state formation in the numerical evaluation of the dark matter relic density for QCD colored dark sectors. Including these non-perturbative effects in the relic density calculation is crucial for achieving accurate predictions in a broad class of models and SE+BSF4DM seamlessly integrates them into the standard micrOMEGAs workflow, requiring minimal user modification. The package is applicable to any model mappable onto a simplified t -channel framework, making it a versatile tool. This paper details the implementation, assets, and scope of SE+BSF4DM, serving as both a comprehensive introduction and a practical user guide.

Keywords: Dark Matter, Sommerfeld Effect, Bound State Formation, Simplified t -channel Models, MicrOmegas, Relic density calculations

PROGRAM SUMMARY

Program title: SE+BSF4DM

Licensing provisions: MIT

Programming language: C++

Github repository: <https://github.com/Nape93-max/SE-BSF4DM>

Nature of the problem: The accurate calculation of the dark matter relic density in models where dark sector particles interact via the strong interaction requires the inclusion of non-perturbative effects, specifically the Sommerfeld effect and bound state formation, which can alter annihilation cross sections by orders of magnitude. While their physical significance is well-established, their implementation has remained highly model-dependent, requiring specialized expertise for each scenario. This has created a gap in the ecosystem of public tools for dark matter phenomenology, as no user-friendly code seamlessly integrates these effects into the standard workflow of popular packages like micrOMEGAs. Consequently, precise phenomenological studies of a broad class of well-motivated models have been hampered by the lack of an accessible and robust public code.

* mathias.becker@unipd.it

† ecopello@uni-mainz.de

‡ martin.napetschnig@tum.de

Solution method: **SE+BSF4DM** computes the relic density by incorporating the Sommerfeld effect and bound state formation for QCD colored dark sector particles through a modular approach into the micrOMEGAs framework. The **Sommerfeld effect** is implemented by numerically extracting the s -wave component of each annihilation cross section. This s -wave part is then multiplied with the appropriate velocity-dependent Sommerfeld factors according to the color decomposition of the process at hand.

For **bound state formation**, the code automatically identifies all possible bound states between (co-)annihilating particles and includes their weighted formation cross sections as additional annihilation channels. This treatment makes use of implemented rates for bound state decay, ionization and transition rate between bound state levels, using analytic expressions available in the literature. The package is applicable to any model with dark sector particles in the (anti-)fundamental representation of $SU(3)_c$.

CONTENTS

Program summary	1
I. Introduction	3
II. Theoretical Framework	4
A. DMSimpt Models	4
B. Long-range effects and their impact on the DM relic density	5
1. Sommerfeld Enhancement	6
2. Bound State Formation including excited states	7
III. Installation and Workflow Integration	9
A. Prerequisites	9
B. Including the SE+BSF4DM package	10
IV. Usage and Examples	10
A. Perturbative Annihilations	10
B. Sommerfeld Effect	11
C. Bound State Formation	13
V. Implementation Details and Performance	14
A. Architecture and micrOMEGAs Integration	14
B. Performance	15
C. Limitations and Future Developments	17
VI. Conclusions	18
Acknowledgements	18
References	19

I. INTRODUCTION

The nature of dark matter (DM) remains one of the outstanding puzzles in particle physics and cosmology. Although weakly interacting massive particles (WIMPs) offer a simple explanation of the observed relic abundance via thermal freeze-out, direct detection and collider searches have placed increasingly strong constraints on the simplest WIMP scenarios [1–6]. These developments have motivated the exploration of more elaborate dark sectors [7, 8], where, for example, several states participate in the thermal freeze-out and coannihilation can play a decisive role. Such frameworks naturally accommodate heavier DM candidates [9–12] and allow a broader range of interactions between the dark sector and the Standard Model (SM).

The increased complexity of these models has driven the development of automated tool chains that compute key DM observables, such as the relic density, direct detection rates, and collider signatures, for a given model of DM [13–17]. One of those tools is micrOMEGAs [13], which, among several other useful functions, efficiently solves the Boltzmann equations for the time-evolution of DM in the early universe. This solution is typically performed considering the perturbative effective annihilation cross section of DM at tree-level. While this approximation is sufficient for many scenarios, it breaks down in the presence of long-range interactions, which can strongly modify the annihilation rate of non-relativistic particles through non-perturbative effects. For example, such effects arise when the dark sector contains particles or mediators carrying SM gauge charges [18–22]. This situation is particularly relevant for QCD-charged states due to the large value of α_s . The *Sommerfeld effect* (SE) [23–28] can significantly enhance or suppress annihilation cross sections, while the radiative formation and decay of *bound states* (BSF) [29–34] opens new, potentially dominant annihilation channels.

Despite their importance, these non-perturbative effects have remained challenging to implement in public numerical tools for the computation of the relic density.¹ While simplified models—particularly *t*-channel DM models (DMSimpt models [35–44])—provide benchmark scenarios with few parameters for studying cosmological and experimental constraints, the community has lacked a user-friendly, publicly available code that seamlessly integrates the SE and BSF into the standard relic density calculation.

To address this gap, we present SE+BSF4DM, a new package for micrOMEGAs that enables the precise calculation of the DM relic density, including both SE and BSF for QCD colored dark sector particles. While particularly suited for DMSimpt models, our package is applicable to any model where dark sector particles transform under the fundamental (or antifundamental) representation of $SU(3)_c$. The code integrates smoothly into the standard micrOMEGAs workflow, requiring minimal user modification while maintaining full compatibility with the code’s existing functionality.

The paper is structured as follows: In section II we outline the theoretical foundations for simplified *t*-channel models and non-perturbative effects. The integration of our package into micrOMEGAs is briefly described in section III. Section IV provides examples of how to use our code, while section V discusses implementation details, performance, and potential future developments. We conclude in section VI.

¹ Ref. [16], implementing SE for the Minimal Supersymmetric Standard Model (MSSM), is a notable exception.

II. THEORETICAL FRAMEWORK

A. DMSimpt Models

In Ref. [38], simplified t -channel DM models (DMSimpt) are introduced with the following Lagrangian:

$$\mathcal{L} = \mathcal{L}_{\text{SM}} + \mathcal{L}_{\text{kin}} + \mathcal{L}_F(\chi) + \mathcal{L}_F(\tilde{\chi}) + \mathcal{L}_S(S) + \mathcal{L}_S(\tilde{S}) + \mathcal{L}_V(V) + \mathcal{L}_V(\tilde{V}) . \quad (1)$$

The first two terms correspond to the SM Lagrangian and to the Gaussian terms of the dark sector, respectively. The remaining six terms describe the interactions that mediate t -channel couplings between the SM and the different DM candidates, namely Dirac and Majorana fermions (\mathcal{L}_F), real and complex scalars (\mathcal{L}_S), and real and complex vectors (\mathcal{L}_V), which we denote in the following by a common generic field X . The characteristic t -channel interactions have the generic structure:

$$\mathcal{L}_{\text{int}} = \lambda X \tilde{Y} \tilde{q} + \text{h.c.} \quad (2)$$

where $\lambda \in \mathbb{C}$; $\tilde{q} = Q_L, u_R, d_R$; $\tilde{Y} = Y^\dagger, \bar{Y}$ in the case of a scalar or fermionic mediator, respectively; and X denotes the DM candidate.² Moreover, we denote with $\delta = (m_Y - m_X)/m_X$ the relative mass splitting in the dark sector. Explicitly one has (denoting scalar and fermionic mediators with φ and ψ , respectively):

$$\mathcal{L}_F(X) = \left[\lambda_{\mathbf{Q}} \bar{X} Q_L \varphi_Q^\dagger + \lambda_{\mathbf{u}} \bar{X} u_R \varphi_u^\dagger + \lambda_{\mathbf{d}} \bar{X} d_R \varphi_d^\dagger + \text{h.c.} \right] , \quad (3)$$

$$\mathcal{L}_S(X) = \left[\hat{\lambda}_{\mathbf{Q}} \bar{\psi}_Q Q_L X + \hat{\lambda}_{\mathbf{u}} \bar{\psi}_u u_R X + \hat{\lambda}_{\mathbf{d}} \bar{\psi}_d d_R X + \text{h.c.} \right] , \quad (4)$$

$$\mathcal{L}_V(X) = \left[\hat{\lambda}_{\mathbf{Q}} \bar{\psi}_Q \gamma^\mu X_\mu Q_L + \hat{\lambda}_{\mathbf{u}} \bar{\psi}_u \gamma^\mu X_\mu u_R + \hat{\lambda}_{\mathbf{d}} \bar{\psi}_d \gamma^\mu X_\mu d_R + \text{h.c.} \right] . \quad (5)$$

All dark sector particles are \mathbb{Z}_2 -odd, ensuring DM stability. The only missing combination in the DMSimpt model is a (Dirac or Majorana) fermionic DM candidate X with a vector mediator Y_μ^a in the fundamental representation of $SU(3)_c$. Apart from a few exceptions [45], vector mediators in the fundamental representation are rarely studied, and this combination is therefore also not implemented in our package. Moreover, renormalizable couplings in the scalar-Higgs sector are not part of the DMSimpt model setup. Such couplings could of course be added, and their perturbative annihilations will be included in the automated relic density calculation by micrOMEGAs.

Scope and application: SE+BSF4DM computes long-range effects for any pair of \mathbb{Z}_2 -odd QCD-colored spin 0 or spin 1/2 particles, making it applicable to the broad class of models mappable onto Eq. (1). While phenomenological studies often consider simplified cases with diagonal, flavor-universal couplings [40], our implementation handles the general scenario. To demonstrate this versatility, we provide three representative examples on [Github](#):

- **F3SuR:** Real scalar DM with fermionic mediator coupling to right-handed up-quarks [36, 46].
- **S3Muni:** Majorana DM with scalar mediator coupling to all right-handed up-type quarks [40].

² The standard DMSimpt implementation uses real Yukawa couplings by default, though complex values are supported.

- **F3W3rd**: Complex vector DM with fermionic mediator to third-generation left-handed quarks.

By automating the inclusion of non-perturbative effects within micrOMEGAs, SE+BSF4DM significantly reduces the computational burden of precisely studying colored dark sectors, enabling a systematic exploration of the parameter space.

The calculation of the dark matter relic density in micrOMEGAs [47] automatically accounts for coannihilation processes through the effective annihilation cross section [9]:

$$\langle \sigma_{\text{eff}} v_{\text{rel}} \rangle = \sum_{\alpha\beta} \langle \sigma_{\alpha\beta} v_{\alpha\beta} \rangle \frac{Y_{\alpha}^{\text{eq}} Y_{\beta}^{\text{eq}}}{\tilde{Y}^{\text{eq}} \tilde{Y}^{\text{eq}}}, \quad (6)$$

$$\tilde{Y}^{\text{eq}} \equiv \sum_{\alpha} Y_{\alpha}^{\text{eq}}, \quad (7)$$

where Y_{α}^{eq} denotes the equilibrium yield of dark sector species α (distinct from the t -channel mediators introduced previously), and $\langle \sigma_{\alpha\beta} v_{\alpha\beta} \rangle$ represents the thermally averaged annihilation cross section for $\alpha + \beta \rightarrow \text{SM particles}$.

B. Long-range effects and their impact on the DM relic density

For models with colored co-annihilators, having strong couplings $\alpha_s \sim \mathcal{O}(0.1) - \mathcal{O}(1)$ necessitates the inclusion of non-perturbative effects [23–34]. Our package modifies $\langle \sigma_{\alpha\beta} v_{\alpha\beta} \rangle$ when both particles α and β are \mathbb{Z}_2 -odd and transform under the **3** or $\bar{\mathbf{3}}$ representation of $SU(3)_c$.

The relevant color decompositions are

$$\mathbf{3} \otimes \bar{\mathbf{3}} = \mathbf{1} \oplus \mathbf{8} \quad (8)$$

$$\mathbf{3} \otimes \mathbf{3} = \bar{\mathbf{3}} \oplus \mathbf{6} \quad (9)$$

$$\bar{\mathbf{3}} \otimes \bar{\mathbf{3}} = \mathbf{3} \oplus \bar{\mathbf{6}}. \quad (10)$$

For sufficiently high energy scales Q , QCD is weakly coupled and described by a long-range Coulomb potential, whose strength and sign depend on the representation $\hat{\mathbf{R}}$:

$$V_{[\hat{\mathbf{R}}]}(r) = -\frac{\alpha_g^{[\hat{\mathbf{R}}]}(Q)}{r}. \quad (11)$$

Here, the effective running coupling $\alpha_g^{[\hat{\mathbf{R}}]}(Q)$ is given by

$$\alpha_g^{[\hat{\mathbf{R}}]}(Q) = \alpha_s(Q) \times \frac{1}{2}[C_2(\mathbf{R}_1) + C_2(\mathbf{R}_1) - C_2(\hat{\mathbf{R}})] \equiv \alpha_s(Q) \times k_{[\hat{\mathbf{R}}]}, \quad (12)$$

where $C_2(\mathbf{R})$ denotes the quadratic Casimirs and $k_{[\hat{\mathbf{R}}]}$ is a representation-dependent prefactor.

For the representations of interest for DMSimpt models, the potentials read as

$$V(r)_{\mathbf{3} \otimes \bar{\mathbf{3}}} = \begin{cases} -\frac{4}{3} \frac{\alpha_s}{r} & [\mathbf{1}] \\ +\frac{1}{6} \frac{\alpha_s}{r} & [\mathbf{8}] \end{cases}, \quad V(r)_{\mathbf{3} \otimes \mathbf{3}} = \begin{cases} -\frac{2}{3} \frac{\alpha_s}{r} & [\bar{\mathbf{3}}] \\ +\frac{1}{3} \frac{\alpha_s}{r} & [\mathbf{6}] \end{cases}. \quad (13)$$

The modified cross section incorporates both Sommerfeld enhancement and bound-state formation:

$$\langle \sigma_{\alpha\beta} v_{\alpha\beta} \rangle = \langle \mathcal{S} \sigma_{\alpha\beta} v_{\alpha\beta} \rangle_{\text{ann}} + \sum_{\substack{\alpha+\beta \rightarrow \mathcal{B}_i \\ \rightarrow \text{SM}}} \langle \sigma_{\text{BSF},i} v_{\text{rel}} \rangle \underbrace{\left(1 - \sum_j (M^{-1})_{ij} \frac{\langle \Gamma_{\text{ion}}^j \rangle}{\langle \Gamma^j \rangle} \right)}_{=:\mathcal{W}_i}. \quad (14)$$

The following subsections detail the implementation of each term in Eq. (14). The first term denotes the Sommerfeld modified annihilation cross section $\langle \mathcal{S} \sigma_{\alpha\beta} v_{\alpha\beta} \rangle_{\text{ann}}$, while the second term is a sum over all the BSF processes of the thermally averaged BSF cross section times the weight factor \mathcal{W}_i accounting for all possible transitions, ionizations and decays.

1. Sommerfeld Enhancement

The first term in Eq. (14) represents the Sommerfeld-corrected annihilation cross section.

\mathcal{S} operates on unaveraged annihilation cross section. Focusing on s-wave contribution, we truncate the series expansion of the cross section in partial waves at zeroth order [48, 49]:

$$\mathcal{S} \sigma_{\alpha\beta} v_{\text{rel}} = \sum_s \sum_{[\mathbf{R}]} c_s^{[\mathbf{R}]} S_0^{[\mathbf{R}]}(\zeta) \sigma_{\alpha\beta}^{(0,s)} v_{\text{rel}} + \mathcal{O}(v_{\text{rel}}^2), \quad (15)$$

where

$$S_0^{[\mathbf{R}]}(\zeta) \equiv S_0 \left(k_{[\mathbf{R}]} \frac{\alpha_s}{v_{\text{rel}}} \right), \quad (16)$$

is the representation-dependent Sommerfeld factor for the s-wave contribution, which is given by

$$S_0(\zeta) = \frac{2\pi\zeta}{1 - e^{-2\pi\zeta}}. \quad (17)$$

In Eq. (15), the velocity expansion extracts the s-wave component in the $v_{\text{rel}} \rightarrow 0$ limit. The coefficients $c_s^{[\mathbf{R}]}$ (with $\sum_s c_s^{[\mathbf{R}]} = 1$) decompose the cross section by final-state spins, as the color decomposition depends on the spin configuration [49]. The running QCD coupling is evaluated at scale $\alpha_s(Q = \mu v_{\text{rel}})$, where μ is the reduced mass of the annihilating pair. The coefficients $k_{[\mathbf{R}]}$ depend on the initial state's color representation according to Eqs. (9) and (8).

We employ a default color decomposition valid for **DMSimpt** models under the assumption $\lambda \ll g_s$, resulting in the following color decompositions [36, 49]:

$$\mathcal{S}\sigma_{\bar{Y}Y \rightarrow g\mathcal{A}} = S_0^{[8]} \sigma_{\bar{Y}Y \rightarrow g\mathcal{A}}, \quad (18)$$

$$\mathcal{S}\sigma_{\bar{Y}Y \rightarrow \mathcal{BC}} = S_0^{[1]} \sigma_{\bar{Y}Y \rightarrow \mathcal{BC}}, \quad (19)$$

$$\mathcal{S}\sigma_{\bar{Y}Y \rightarrow gg} = \left(\frac{2}{7} S_0^{[1]} + \frac{5}{7} S_0^{[8]} \right) \sigma_{XX^\dagger \rightarrow gg}, \quad (20)$$

$$\mathcal{S}\sigma_{\bar{Y}_i Y_j \rightarrow \bar{q}_i q_j} = \sigma_{\bar{Y}_i Y_j \rightarrow \bar{q}_i q_j} \times \begin{cases} S_0^{[8]}, Y \text{ fermionic} \ \& \ i = j \\ \frac{1}{9} S_0^{[1]} + \frac{8}{9} S_0^{[8]}, \text{ else} \end{cases}, \quad (21)$$

$$\mathcal{S}\sigma_{Y_i Y_j \rightarrow q_i q_j} = \sigma_{Y_i Y_j \rightarrow q_i q_j} \times \begin{cases} S_0^{[6]}, Y \text{ scalar} \ \& \ i = j \\ \frac{1}{3} S_0^{[3]} + \frac{2}{3} S_0^{[6]}, \text{ else} \end{cases}. \quad (22)$$

Here, \mathcal{A} in Eq. (18) denotes color-neutral SM vector bosons $\{A, W^\pm, Z\}$, while \mathcal{B} and \mathcal{C} in Eq. (19) represent any color-neutral SM particles $\{A, W^\pm, Z, h, \ell\}$. The indices i, j in Eqns. (21) and (22) label quark and mediator flavors.

Users may modify the coefficients $c_s^{[\mathbf{R}]}$ for scenarios such as $\lambda \gg g_s$, with implementation details provided in Sec. IV B and Listing 2. A more detailed discussion on the physics of these decompositions (related to the symmetry of the overall wavefunction) will be given in a companion paper [46].

We implement the Sommerfeld effect for colored annihilating particles in three steps:

1. Taylor expansion in velocity to extract the v_{rel}^0 contribution.
2. Color decomposition for initial states in $\mathbf{3} \otimes \mathbf{3}$, $\mathbf{3} \otimes \bar{\mathbf{3}}$, or $\bar{\mathbf{3}} \otimes \bar{\mathbf{3}}$.
3. Enhancement/suppression factor following Eqns. (18)-(22).

These steps are implemented using micrOMEGAs' built-in `improveCrossSection` method (see Sec. V), with the resulting improved cross section undergoing standard thermal averaging.

2. Bound State Formation including excited states

The second term in Eq. (14) accounts for bound-state formation (BSF), where annihilating particles in a $\mathbf{3} \otimes \bar{\mathbf{3}}$ color configuration form hydrogen-like metastable bound states \mathcal{B}_i with quantum numbers $i = \{n, \ell, m, s\}$ that subsequently decay into Standard Model particles. This represents an additional annihilation channel beyond the Sommerfeld-enhanced perturbative processes. The derivation of the effective cross section in Eq. (14) follows Refs. [50, 51].

The weight factor \mathcal{W}_i in Eq. (14),

$$\mathcal{W}_i = 1 - \sum_j (M^{-1})_{ij} \frac{\langle \Gamma_{\text{ion}}^j \rangle}{\langle \Gamma^j \rangle}, \quad (23)$$

accounts for ionization by thermal particles ($\langle \Gamma_{\text{ion}}^i \rangle$), decay into gluons ($\langle \Gamma_{\text{dec}}^i \rangle$), and transitions between bound-state levels ($\langle \Gamma_{\text{trans}}^{i \rightarrow j} \rangle$) mediated by SM photons.³ The matrix M and the rate $\langle \Gamma^i \rangle$

³ In `DMSimpt` models, mediators carry electric charge by construction. The strong interaction cannot mediate transitions.

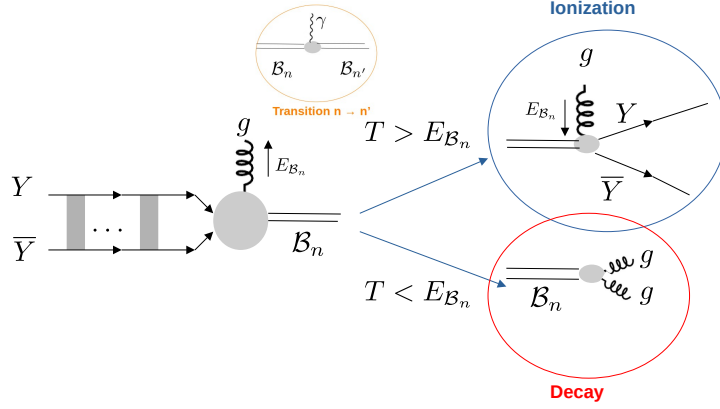


FIG. 1: Schematic BSF process with ionization, decay, and transitions.

in Eq. (14) are defined as [51]:

$$M_{ij} \equiv \delta_{ij} - \frac{\langle \Gamma_{\text{trans}}^{i \rightarrow j} \rangle}{\langle \Gamma^i \rangle}, \quad (24)$$

$$\langle \Gamma^i \rangle = \langle \Gamma_{\text{ion}}^i \rangle + \langle \Gamma_{\text{dec}}^i \rangle + \sum_{j \neq i} \langle \Gamma_{\text{trans}}^{i \rightarrow j} \rangle. \quad (25)$$

The various processes are illustrated in Fig. 1.

The matrix M has dimension $((2s+1)n^2)^2$ when including states up to principal quantum number n , leading to $\mathcal{O}(n^4)$ scaling that significantly impacts computational performance (see Section VB). To ensure the validity of the Coulomb potential, we require binding energies $E_{B_i} = \frac{\mu(\alpha_b^{(i)})^2}{2n^2} \gtrsim \Lambda_{\text{QCD}}$, yielding $n \lesssim 20$ for $\mathcal{O}(1 \text{ TeV})$ masses, where Λ_{QCD} is the QCD confinement scale and $\alpha_b^{(i)}$ is the strong coupling constant evaluated at the Bohr momentum of bound state i .

We implement the rates from Ref. [52] for $\sigma_{\text{BSF},i} v_{\text{rel}}$, computing thermal averages using micrOMEGAs' Simpson integration.⁴ The full BSF contribution is added to the effective cross section via micrOMEGAs' `darkOmegaExt` routine. Users may select from four computational schemes:

⁴ Ref. [53] provides equivalent updated expressions. Unitarity issues raised in Refs. [52, 53] are negligible for $n \lesssim 20$.

1. **No Transition Limit:** Neglects inter-state transitions, considering only $\ell = 0$ states. This provides an excellent approximation for **DMSimpt** models given $\alpha_{\text{QED}} \ll \alpha_s$:

$$\langle \sigma_{\text{BSF}} v_{\text{rel}} \rangle_{\text{eff}} = \sum_i \langle \sigma_{\text{BSF},i} v_{\text{rel}} \rangle \frac{\langle \Gamma_{\text{dec}}^i \rangle}{\langle \Gamma_{\text{dec}}^i \rangle + \langle \Gamma_{\text{ion}}^i \rangle}. \quad (26)$$

2. **Efficient Transition Limit:** Assumes rapid de-excitation to $\ell = 0$ states, including all bound states:

$$\langle \sigma_{\text{BSF}} v_{\text{rel}} \rangle_{\text{eff}} = \left(\sum_i \langle \sigma_{\text{BSF},i} v_{\text{rel}} \rangle \right) \frac{\Gamma_{\text{dec}}^{\text{eff}}}{\Gamma_{\text{dec}}^{\text{eff}} + \Gamma_{\text{ion}}^{\text{eff}}}, \quad (27)$$

$$\Gamma_{\text{ion/dec}}^{\text{eff}} \equiv \frac{\sum_i \langle \Gamma_{\text{ion/dec}}^i \rangle Y_{\mathcal{B}_i}^{\text{eq}}}{\sum_j Y_{\mathcal{B}_j}^{\text{eq}}}. \quad (28)$$

In Eq. (28) above, $Y_{\mathcal{B}_i}^{\text{eq}}$ denote the equilibrium yields of bound state species i .

3. **Ionization Equilibrium:** Represents the theoretical maximum. Typically realized at high temperatures but tends to strongly overestimate $\langle \sigma_{\text{BSF}} v_{\text{rel}} \rangle_{\text{eff}}$ at lower temperatures:

$$\langle \sigma_{\text{BSF}} v_{\text{rel}} \rangle_{\text{eff}} = \frac{1}{g_{Y_1} g_{Y_2}} \left(\frac{2\pi}{T\mu} \right)^{3/2} \sum_i g_{\mathcal{B}_i} e^{E_{\mathcal{B}_i}/T} \Gamma_{\text{dec}}^i, \quad (29)$$

where $g_{Y_i}, g_{\mathcal{B}_i}, E_{\mathcal{B}_i}$ denote, respectively, the degrees of freedom of the bound state forming particles, the bound state itself and its binding energy. As before, μ denotes the effective mass.

4. **Full Matrix Solution:** Implements the full expression from Eq. (14).

III. INSTALLATION AND WORKFLOW INTEGRATION

A. Prerequisites

Although the preparation of a CalcHEP model file is not directly related to our package, we provide a brief summary of the workflow here to ensure self-containment.

The workflow to generate the necessary model files is as follows:

1. **Model customization:** The FeynRules file `dmsimpt_v1.2.fr` provided on the [DMSimpt page](#) should be customized, i.e., extract only the terms relevant for the specific t -channel model at hand.
2. **CalcHEP output generation:** The Mathematica notebook `use-DMSimpt.nb` (also available on the [DMSimpt page](#) [54]) is used to generate the CalcHEP output for micrOMEGAs.⁵
3. **Example files:** The specific FeynRules and CalcHEP files for the three benchmark models discussed in this work can be found in the [🔗 Examples_Tutorial/FeynRules_CalcHEP](#) directory of our GitHub repository.

⁵ A brief technical note: The notebook `use-DMSimpt.nb` works as expected with Mathematica 14.0 and older versions, but throws several errors when executed with Wolfram 14.3. The resolution of this compatibility issue is deferred to experts.

B. Including the SE+BSF4DM package

To use SE+BSF4DM, micromEGAs version 6.0. or higher has to be installed in the usual manner. The package is then included by copying the `copy_into_Packages/SE_BSF` directory, available on our [GitHub page](#), into the `micromegas_6.2.4/Packages/` directory. These files contain the model-independent core functionalities of our package. Note that this action alone does not modify standard micromEGAs behavior; the SE+BSF effects are only activated when explicitly enabled for a specific model.

To integrate our package for a certain model, the following steps have to be performed:

1. Initialization of a new model by using the standard micromEGAs command `./newProject MODEL`.
2. The CalcHEP model files `extlib1.mdl`, `func1.mdl`, `lgrng1.mdl`, `prtcls1.mdl` and `vars1.mdl`, which have been created as detailed in Sec. III A, have to be transferred in to the `micromegas_6.2.4/MODEL/work/models/` directory of the newly generated model (e.g. `S3Muni`).
3. To enable the inclusion of SE and BSF in the freshly generated model, the two model-specific files `improveCrossSection_Sommerfeld.cpp` and `BoundStateFormation.cpp`, contained in the `copy_into_MODEL_lib/` directory in our [GitHub repository](#), should be transferred into the `micromegas_6.2.4/MODEL/lib/` folder.

The final step is to configure these model-specific files, a process detailed in the following section.

IV. USAGE AND EXAMPLES

A. Perturbative Annihilations

Before activating any non-perturbative effects, the foundational step is to integrate the model-specific files `lib/improveCrossSection_Sommerfeld.cpp` and `lib/BoundStateFormation.cpp` into the micromEGAs build. This is done by including them in the `main.cpp` file of your model directory, as shown in Listing 1.

```

1/* #include "../include/micromegas.h"
2#include "../include/micromegas_aux.h"
3If our SE+BSF4DM is used, these two files are included directly in
4"lib/improveCrossSection_Sommerfeld.cpp" and "lib/BoundStateFormation.
   cpp" */
5#include "lib/pmodel.h"
6#include "lib/improveCrossSection_Sommerfeld.cpp"
7#include "lib/BoundStateFormation.cpp"

```

Listing 1: Files to be included in the `main.cpp` file in micromEGAs.

With these files included but the key configuration flags—`somm_flag` in `lib/improveCrossSection_Sommerfeld.cpp` and `bsf_scenario` in `lib/BoundStateFormation.cpp`—set to zero, the relic density is computed using the standard perturbative cross sections.

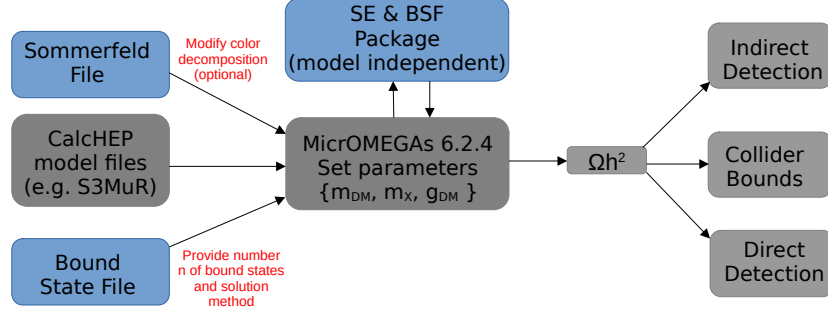


FIG. 2: Schematic workflow of the SE+BSF4DM package.

B. Sommerfeld Effect

To activate the Sommerfeld enhancement, users must set `somm_flag = 1` in `lib/improveCrossSectionSommerfeld.cpp`. The implementation calculates velocity-dependent enhancement factors for annihilation channels by decomposing the initial state into irreducible color representations.

The relevant color decompositions for `DMSimpt` models are pre-implemented under the assumption that the t -channel coupling $\lambda \ll g_s$, requiring no modification for standard use cases.⁶

The core computation takes place in the function `SommerfeldFactorBSMmodel`, where the color decomposition is handled through conditional `if...else` blocks that identify specific initial and final states. Listing 2 shows the key implementation, with coefficients `kQfac1`, `kQfac3`, `kQfac6`, and `kQfac8` corresponding to the representations **1**, **3**, **6** and **8**, respectively (if unspecified, `kQfac = 0`).

⁶ In the opposite regime $\lambda \gg g_s$, coannihilations become less important, as the processes $XX \rightarrow qq$ dominate.

```

1 // *** BEGIN IF BLOCK OF COLOR DECOMPOSITION (CAN BE MODIFIED
  OPTIONALLY) ***
2 if((c1==3&&c2==-3)|| (c1==-3&&c2==3)){ // Y Ybar process
3     if((c3!=8&&c4==8)|| (c3==8&&c4!=8)){ //g + Z/\gamma.
4         // This is purely adjoint for all partial waves.
5         kQfac8=1.;
6     }
7     if(c3==1&&c4==1){ // most frequent case: Both final states are colour
        singlets
8         kQfac1=1.; //for all partial waves
9     }
10    if(c3==8&&c4==8){ //gg final state
11        kQfac1=2./7.; kQfac8=5./7.; //gg channel
12    }
13    if((c3==3&&c4==3)|| (c3==3&&c4==3)){ //q qbar final state
14        /* This is the tricky channel, as elaborated in our publication.
15        Interference terms in the color decomposition are neglected */
16        if((s1==1 && s2==1)&&(n3 == -n4)){
17            // fermionic mediators and identical quark flavors in the final
18            state
19            kQfac8=1.; // for all partial waves in the case \lambda << g_s
20        }
21        else{ // different quark flavors in the final state or scalar
22            mediators
23            kQfac1=1./9.; kQfac8=8./9.;
24            //for all partial waves in the case \lambda << g_s
25        }
26    }
27    if((c1==3&&c2==3)|| (c1==-3&&c2==3)){ // q_i q_j or q_i_bar, q_j_bar
        final state
28        if((s1==0 && s2==0)&&(n3==n4)) {
29            // Scalar mediators and equal quark flavors in the final state
30            kQfac6=1.;
31        }
32        else {
33            kQfac3=1./3.; kQfac6=2./3.;
34        }
35    }
36 // *** END IF BLOCK OF COLOR DECOMPOSITION ***

```

Listing 2: Color decomposition implementation for Sommerfeld enhancement in `lib/improveCrossSectionSommerfeld.cpp`. The complete block handles all relevant initial/final state combinations for DMSimpt models.

The theoretical foundation for these color decompositions is detailed in Section IIB1, where the specific coefficients `kQfac` (corresponding to $c_s^{[R]}$) are stated. For example, line 11 in Listing 2 describes the process $\bar{Y}Y \rightarrow gg$ (see Eq. (20)), while line 32 describes the process $Y_i Y_j \rightarrow q_i q_j$, $i \neq j$ (see Eq. (22)) for different flavors of mediators.

Advanced users may implement their custom color decomposition, Sommerfeld corrections to higher partial waves or loop-improved cross sections by setting `somm_flag = 2` and modifying the user-defined block at the end of the `improveCrossSection` function, maintaining compatibility with micrOMEGAs' original purpose for this function. While micrOMEGAs contain built-in Sommerfeld functions optimized for massive force mediators [55], our package employs analytic expressions for the QCD Coulomb potential featuring massless force mediators (gluons).

C. Bound State Formation

To activate BSF, users must provide two inputs: the number of excited states that they wish to be considered and the solution method, see Sec. IIB2.

Configuration: In `lib/BoundStateFormation.cpp`, users specify the treatment of bound states via the `bsf_scenario` flag and the number of excited states via `num_excited_states`, as shown in Listing 3. The available scenarios, detailed in Section IIB2, are the computationally efficient **No Transition** limit (1), the **Efficient Transition** limit (2), the **Ionization Equilibrium** (3), and the **Full Matrix** solution (4). In simplified t -channel models, scenario 1 provides an excellent approximation to the full solution.

```

1#include"../../Packages/SE_BSF/SE_BSF_header.h"
2#include"../../Packages/SE_BSF/SE_BSF_functions.cpp"
3/* In this file, the user has to supply some details of the model for BSF.
   The following information needs to be provided:
4 1) The BSF scenario/limit
5 2) The number of excited states to be considered */
6int bsf_scenario = 1; //Flag for BSF (0 = no BSF, 1 = no transition limit,
   2 = efficient transition limit, 3 = ionization equilibrium, 4 = Full
   matrix solution)
7int num_excited_states = 1; //Number of n states included in the
   calculation (n = 0 -> no bound states, n = 1 -> ground state etc.)
8// *** END USER DEFINITION ***

```

Listing 3: User defined settings in the `lib/BoundStateFormation.cpp` file for activating and controlling bound-state effects.

Integration: The final step replaces the standard relic density calculation in `main.cpp` with the extended version that includes bound-state effects, as shown in Listing 4.

```

1 if(Ncdm==1)
2 {   double Xf;
3     //Omega=darkOmega(&Xf,fast,Beps,&err); //Conventional MO calculation
        without BSF
4     Omega = darkOmegaExt(&Xf, BSF_XS_A, BSF_XS_S); // MO calculation with
        BSF
5     printf("Xf=%.2e Omega=%.2e\n",Xf,Omega);
6     if(Omega>0)printChannels(Xf,cut,Beps,1,stdout);}

```

Listing 4: Usage of `darkOmegaExt` in the `main.cpp` file to include (excited) bound state effects.

Comparison of bound-state solution methods: Figure 3 demonstrates the different methods for obtaining the effective cross section for the F3SuR model with degenerate masses between DM and the Dirac mediator ($\delta = 0$). The gray baseline shows the purely perturbative cross section, while the red curve includes SE. The **Full matrix** solution, including $n = 15$ bound state levels (solid black), represents the most complete treatment. For physical consistency, we restrict $n \leq 20$, ensuring the binding energy is always above the QCD scale for TeV-scale mediators. The dotted **Ionization equilibrium** curve represents the theoretical maximum possible enhancement. The **No transition** approximation (dashed black) provides excellent agreement with the full solution at freeze-out temperatures ($x \sim 20 - 30$) with significantly lower computational cost, while the **Efficient transition** method (dash-dotted) overestimates the cross section. It could be used to obtain conservative upper bounds on $\langle \sigma_{\text{BSF}v} \rangle_{\text{eff}}$.

The colored lines show contributions from individual principal quantum numbers ($n = 1 - 5$) using the **Full matrix** solution. At freeze-out, the ground state ($n = 1$) dominates, while excited states become increasingly important at later times. The dash-dot-dotted lines show spin-triplet contributions, which are suppressed at freeze-out by small decay widths but dominate at low temperatures due to a statistical factor stemming from the spin sum in the cross section.

Excited states and dependence on mass splitting: The late-time enhancement from excited states ($n > 1$) and spin-triplets is strongly suppressed by non-zero mass splitting $\delta > 0$ between dark matter and co-annihilating partners, as the effective cross section experiences an additional $e^{-2x\delta}$ suppression. As shown in Fig. 4, bound-state effects are therefore most pronounced for nearly degenerate spectra ($\delta \lesssim 0.01$), making bound-state effects particularly relevant for models with small mass splittings or models where the DM candidate itself is color-charged.

For advanced users, the `darkOmegaExt` interface also allows implementation of custom cross section enhancements by replacing the final two arguments of `darkOmegaExt` with user-defined functions, maintaining full compatibility with the original functionality.

V. IMPLEMENTATION DETAILS AND PERFORMANCE

A. Architecture and micrOMEGAs Integration

The implementation of non-perturbative effects leverages and extends micrOMEGAs' existing infrastructure while maintaining computational efficiency.

Sommerfeld effect: The enhancement is computed by numerically extracting the leading order term in the Taylor expansion of the micrOMEGAs-internally computed $\sigma_{\text{ann}} v_{\text{rel}}(v_{\text{rel}})$, which

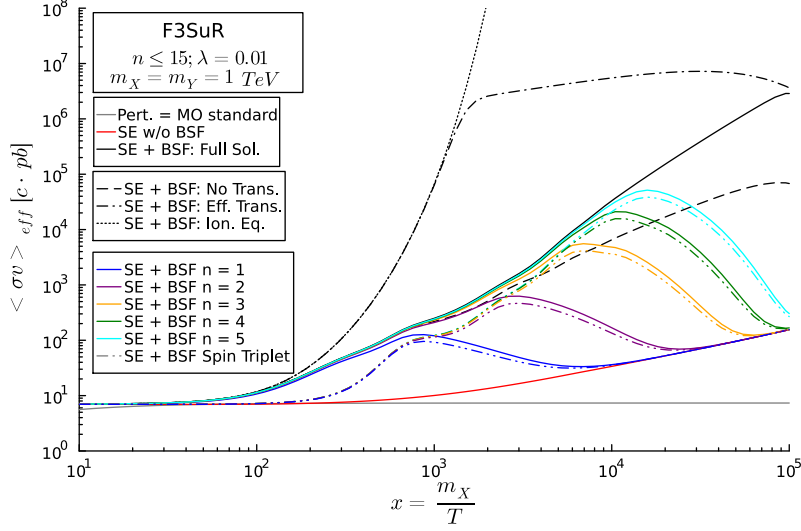


FIG. 3: Comparison of effective cross sections for different bound-state treatment methods in the F3SuR model with mass degeneracy ($\delta = 0$). Colors indicate contributions from different principal quantum numbers n using the full matrix solution.

coincides with the s-wave contribution in the limit $v_{\text{rel}} \rightarrow 0$.⁷ Depending on the color charge of the particles in the initial and final states, the appropriate color decomposition (which can be straightforwardly modified by the user) is employed, as described in Sec. II B 1 and Listing 2.

Bound state formation: The package computes the total effective cross section by summing micrOMEGAs’ standard annihilation channels (potentially including Sommerfeld enhancement) with all relevant bound-state formation processes. Ionization and decay rates are taken from Ref. [51], while BSF and transition rates are taken from Ref. [52]. It is well known [33, 56] that the running coupling α_s that enters in the BSF and decay rates is evaluated at different scales, sometimes these values need to be self-consistently solved numerically, e.g. the coupling at the scale of the Bohr momentum $\alpha_b^{(i)} = \alpha_s(Q = \mu\alpha_b^{(i)})$. The calculation employs micrOMEGAs’ built-in function `alphaQCD(Q)` for the strong running coupling and obtains $\alpha_b^{(i)}$ numerically via the Newton-Raphson method [57]. The `simpsonArg` routine is used for thermal averaging the BSF rates. For the **Full matrix** solution, the matrix M containing all the transition rates is diagonalized using micrOMEGAs’ internal `rDiagonalA` diagonalization routine.

B. Performance

To quantify the computational cost of including non-perturbative effects, we conducted a series of performance benchmarks. All timing measurements were performed on a desktop workstation

⁷ This approach can not be extended to the p-wave, due to inseparable mixing between s- and p-wave contributions in the v_{rel}^2 term in the expansion.

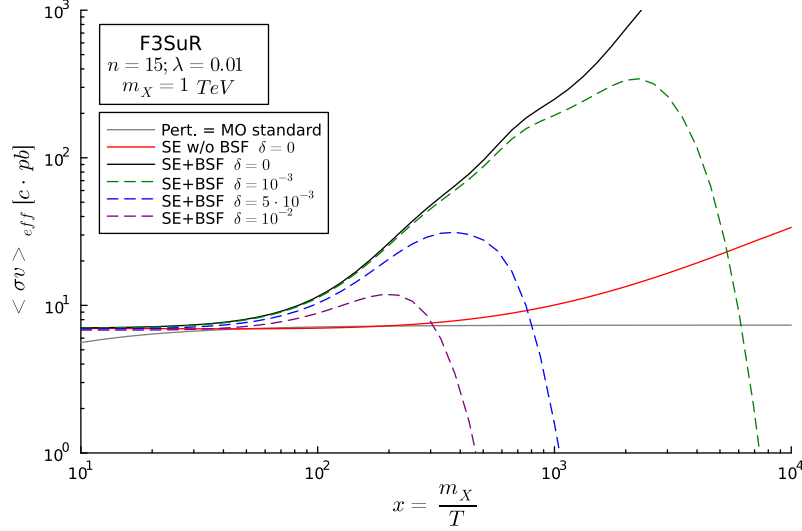


FIG. 4: Dependence of the bound-state enhanced cross section on mass splitting δ in the F3SuR model. Smaller splittings allow longer-lived co-annihilation, enhancing late-time bound-state formation.

with an Intel Core i7-12700K processor and 16 GB of RAM, running Ubuntu 20.04 LTS. The code was compiled and executed using the standard micrOMEGAs 6.2.4 build system. Reported runtimes represent the average real time over 100 executions for each configuration.

The performance of SE+BSF4DM is highly model-dependent, influenced by factors such as mediator masses (relative to the DM mass), the number of mediator species, and their spins. For this study, we present benchmarks for the F3SuR model with a Dirac fermionic mediator and a mass splitting of $\delta = 10^{-2}$.

Table I summarizes the results. The columns correspond to the possible choices for `bsf_scenario`, introduced in Sec. IV C. The benchmark value is the runtime of a standard micrOMEGAs calculation with the `darkOmega` method, not making use of SE+BSF4DM. Sommerfeld enhancement can be used both with `darkOmega` and `darkOmegaExt`, whereas BSF is only included when using `darkOmegaExt`.

Including the Sommerfeld effect alone introduces a negligible computational overhead compared to the perturbative calculation. Adding the ground-state ($n = 1$) bound state contribution also has a minimal impact. However, the runtime increases significantly when including excited states ($n > 1$), with the scaling behavior strongly dependent on the method used to solve the network of Boltzmann equations:

The efficient transition limit (**Eff. Tran**), where all ℓ bound state levels contribute, scales approximately as $\mathcal{O}(n^2)$. The **Full Matrix** method, diagonalizing the matrix M in Eq. (14) by computing all QED mediated $\ell \rightarrow \ell'$ transitions, scales as $\mathcal{O}(n^4)$, becoming computationally intensive for large n . We restrict our analysis to $n \leq 20$, as for higher principal quantum numbers the binding energy E_{B_n} falls below Λ_{QCD} for dark matter masses below ~ 10 TeV, rendering the weakly coupled bound state picture invalid. The ionization equilibrium (**Ion. Eq.**) approximation becomes unphysical at

low temperatures, and the cross sections become excessively large (as theoretically expected).

In summary, while our implementation of the Sommerfeld effect introduces minimal overhead, the user’s choice regarding the treatment of excited bound states is the primary determinant of computational cost. As can be seen in Fig. 3, the computationally fast no transition limit (**No Tran.**) is a good approximation for the **Full Matrix** solution in the low x -region (which is the relevant one for coannihilation).

C. Limitations and Future Developments

SE+BSF4DM is designed to be accessible and follows the logical structure of micrOMEGAs, ensuring ease of use. However, several avenues for future improvement and current limitations should be discussed:

Extension to conversion-driven freeze-out and Super-WIMP: The most significant potential improvement concerns the treatment of conversion-driven freeze-out (cospin) regimes of parameter space [58, 59], which exhibit a very small t -channel coupling λ ($\mathcal{O}(10^{-9} - 10^{-7})$), spoiling chemical equilibrium in the dark sector.

The SE and BSF improved annihilation rates are implemented assuming chemical equilibrium and the standard coannihilation scenario to hold, where excited states provide only subleading corrections. However, as demonstrated, excited states play a pivotal role in conversion-driven freeze-out [51] and in the Super-WIMP scenario [52].

The implementation of this functionality is conceptually straightforward within our framework and would leverage micrOMEGAs’ existing formalism for N -component dark matter [55]. This extension would merely require the future availability of a `darkOmegaNext` function, which would unify the features of the currently available functions `darkOmegaN` and `darkOmegaExt`. We are in contact with the micrOMEGAs developers, and this will be the focus of a follow-up work.

Once available, combining `darkOmegaNext` with SE+BSF4DM would enable automated relic density predictions in this regime, which is also experimentally interesting for long-lived particle searches at colliders [42].

Numerical optimization of the ‘Full Matrix’ solution: We currently use micrOMEGAs’ internal mass diagonalization routine `rDiagonalA` for computing M^{-1} in Eq. (14), specifically by diagonalizing $M \rightarrow U^\dagger M_D U$ and computing its inverse via $M^{-1} = U M_D^{-1} U^\dagger$. The matrix inversion represents the most computationally intensive part of this solution method at the moment.

Color representations: The applicability of our package to `DMSimpt` models stems from the fact that these models feature colored particles exclusively in the $\mathbf{3}$ or $\bar{\mathbf{3}}$ representations of $SU(3)_c$. Consequently, the implemented Sommerfeld effect is restricted to $\mathbf{3} \otimes \mathbf{3}$ and $\bar{\mathbf{3}} \otimes \mathbf{3}$ processes, while BSF is currently limited to the $\bar{\mathbf{3}} \otimes \mathbf{3}$ channels.⁸

Extending SE+BSF4DM to other representations, such as color-octet mediators, would allow to study a larger class of models, but also require more involved color decompositions for both the SE and BSF.

⁸ In Ref. [40] it has been shown that the impact of $\mathbf{3} \otimes \mathbf{3}$ bound states have a negligible impact if the two particles forming bound states have equal mass.

TABLE I: Performance benchmarks of the different methods used in SE+BSF4DM for the F3SuR model.

Process	Runtime (seconds)				
	No BSF	No Tran.	Eff. Tran.	Ion. Eq.	Full Matrix
<i>Baseline</i>					
Perturbative (<code>darkOmega</code>)	0.04	–	–	–	–
SE only (<code>darkOmega</code>)	0.05	–	–	–	–
Perturbative (<code>darkOmegaExt</code>)	0.06	–	–	–	–
SE only (<code>darkOmegaExt</code>)	0.07	–	–	–	–
SE + BSF $n = 1$ (ground state)	–	0.07	0.07	–	0.07
<i>Excited states</i>					
SE + BSF $n = 2$	–	0.08	0.09	0.07	0.09
SE + BSF $n = 3$	–	0.10	0.11	0.07	0.11
SE + BSF $n = 4$	–	0.11	0.14	0.08	0.17
SE + BSF $n = 5$	–	0.12	0.20	0.08	0.26
SE + BSF $n = 20$	–	0.72	6.70	–	98.00

VI. CONCLUSIONS

We have presented SE+BSF4DM, a new package for micrOMEGAs that enables the calculation of the dark matter relic density including the Sommerfeld effect and bound-state formation for QCD-colored particles. The package requires minimal modification from the user and integrates seamlessly into the standard micrOMEGAs workflow without interfering with its other functionalities. It is applicable to a class of well-motivated models, rendering it a versatile tool.

While this article is intended to serve as a self-contained guide for the SE+BSF4DM package, the phenomenological impact of these effects, including a comprehensive analysis of the relic density and experimental constraints, is explored in a separate work [46].

A key assumption in the current implementation is the maintenance of chemical equilibrium within the dark sector. As discussed, a particularly promising development is the treatment of conversion-driven freeze-out, which could be readily implemented upon the future availability of the proclaimed `darkOmegaExt` function in a future release of micrOMEGAs.

We hope that SE+BSF4DM will become a valuable tool for the community and that the inclusion of Sommerfeld and bound-state effects will become the new standard in the computation of relic densities for dark sectors with QCD-charged particles, ultimately leading to more robust and accurate experimental exclusion bounds.

ACKNOWLEDGEMENTS

We thank Alexander Pukhov for his support during the implementation in micrOMEGAs, and Pablo Olgoso for feedback on the draft.

M. N thanks Merlin Reichard and Julian Mayer-Steudte for useful input on the code and Stefan Lederer for fruitful discussions. M. B. and E. C. acknowledge support from the Emmy Noether Grant No. HA 8555/1-1 funded by the Deutsche Forschungsgesellschaft (DFG). E. C. and M. N. acknowledge support from the DFG Collaborative Research Centre “Neutrinos, Dark Matter and

Messengers” (SFB 1258). M. B., E. C. acknowledge support by the Cluster of Excellence ”Precision Physics, Fundamental Interactions, and Structure of Matter” (PRISMA⁺ EXC 2118/1) funded by the DFG within the German Excellence Strategy (project No. 390831469). This work was supported by Istituto Nazionale di Fisica Nucleare (INFN) through the Theoretical Astroparticle Physics (TAsP) project, and in part by the Italian MUR Departments of Excellence grant 2023-2027 “Quantum Frontiers”. The work of M.B. was supported in part by the Italian Ministry of University and Research (MUR) through the PRIN 2022 project n. 20228WHTYC (CUP:I53C24002320006 and C53C24000760006).

-
- [1] J. Aalbers *et al.* (LZ), *Phys. Rev. Lett.* **131**, 041002 (2023), [arXiv:2207.03764 \[hep-ex\]](#).
 - [2] E. Adams *et al.* (PICO), *Phys. Rev. D* **108**, 062003 (2023), [arXiv:2301.08993 \[astro-ph.CO\]](#).
 - [3] E. Aprile *et al.* (XENON), *Eur. Phys. J. C* **84**, 784 (2024), [arXiv:2402.10446 \[physics.ins-det\]](#).
 - [4] G. Arcadi, M. Dutra, P. Ghosh, M. Lindner, Y. Mambrini, M. Pierre, S. Profumo, and F. S. Queiroz, *Eur. Phys. J. C* **78**, 203 (2018), [arXiv:1703.07364 \[hep-ph\]](#).
 - [5] T. Abe *et al.* (LHC Dark Matter Working Group), *Phys. Dark Univ.* **27**, 100351 (2020), [arXiv:1810.09420 \[hep-ex\]](#).
 - [6] G. Aad *et al.* (ATLAS), *Sci. Bull.* **69**, 3005 (2024), [arXiv:2306.00641 \[hep-ex\]](#).
 - [7] P. Harris, P. Schuster, and J. Zupan, in *Snowmass 2021* (2022) [arXiv:2207.08990 \[hep-ph\]](#).
 - [8] M. Cirelli, A. Strumia, and J. Zupan, *Dark matter* (2024), [arXiv:2406.01705 \[hep-ph\]](#).
 - [9] K. Griest and D. Seckel, *Phys. Rev. D* **43**, 3191 (1991).
 - [10] P. Gondolo and G. Gelmini, *Nucl. Phys. B* **360**, 145 (1991).
 - [11] J. Harz, B. Herrmann, M. Klasen, K. Kovarik, and Q. L. Boulc’h, *Phys. Rev. D* **87**, 054031 (2013), [arXiv:1212.5241 \[hep-ph\]](#).
 - [12] M. J. Baker *et al.*, *JHEP* **12**, 120, [arXiv:1510.03434 \[hep-ph\]](#).
 - [13] G. Belanger, F. Boudjema, A. Pukhov, and A. Semenov, *Comput. Phys. Commun.* **176**, 367 (2007), [arXiv:hep-ph/0607059](#).
 - [14] T. Bringmann, J. Edsjö, P. Gondolo, P. Ullio, and L. Bergström, *JCAP* **07**, 033, [arXiv:1802.03399 \[hep-ph\]](#).
 - [15] F. Ambrogio, C. Arina, M. Backovic, J. Heisig, F. Maltoni, L. Mantani, O. Mattelaer, and G. Mohlabeng, *Phys. Dark Univ.* **24**, 100249 (2019), [arXiv:1804.00044 \[hep-ph\]](#).
 - [16] J. Harz, B. Herrmann, M. Klasen, K. Kovarik, and L. P. Wiggeling, *Eur. Phys. J. C* **84**, 342 (2024), [arXiv:2312.17206 \[hep-ph\]](#).
 - [17] M. Palmiotta, A. Arbey, and F. Mahmoudi, *Comput. Phys. Commun.* **294**, 108905 (2024), [arXiv:2211.10376 \[hep-ph\]](#).
 - [18] J. Ellis, K. A. Olive, and J. Zheng, *Eur. Phys. J. C* **74**, 2947 (2014), [arXiv:1404.5571 \[hep-ph\]](#).
 - [19] A. Ibarra, A. Pierce, N. R. Shah, and S. Vogl, *Phys. Rev. D* **91**, 095018 (2015), [arXiv:1501.03164 \[hep-ph\]](#).
 - [20] S. El Hedri, A. Kaminska, M. de Vries, and J. Zurita, *JHEP* **04**, 118, [arXiv:1703.00452 \[hep-ph\]](#).
 - [21] S. El Hedri and M. de Vries, *JHEP* **10**, 102, [arXiv:1806.03325 \[hep-ph\]](#).
 - [22] S. Biondini and S. Vogl, *JHEP* **11**, 147, [arXiv:1907.05766 \[hep-ph\]](#).
 - [23] A. Sommerfeld, *Annalen Phys.* **403**, 257 (1931).
 - [24] A. D. Sakharov, *Zh. Eksp. Teor. Fiz.* **18**, 631 (1948).
 - [25] M. Beneke, C. Hellmann, and P. Ruiz-Femenia, *JHEP* **03**, 162, [arXiv:1411.6930 \[hep-ph\]](#).
 - [26] M. Beneke, R. Szafron, and K. Urban, *Phys. Lett. B* **800**, 135112 (2020), [arXiv:1909.04584 \[hep-ph\]](#).
 - [27] J. Hisano, S. Matsumoto, M. Nagai, O. Saito, and M. Senami, *Phys. Lett. B* **646**, 34 (2007), [arXiv:hep-ph/0610249](#).
 - [28] J. Branahl, J. Harz, B. Herrmann, M. Klasen, K. Kovarik, and S. Schmiemann, *Phys. Rev. D* **100**, 115003 (2019), [arXiv:1909.09527 \[hep-ph\]](#).
 - [29] B. von Harling and K. Petraki, *JCAP* **12**, 033, [arXiv:1407.7874 \[hep-ph\]](#).

- [30] J. Ellis, F. Luo, and K. A. Olive, *JHEP* **09**, 127, [arXiv:1503.07142 \[hep-ph\]](#).
- [31] H. An, M. B. Wise, and Y. Zhang, *Phys. Rev. D* **93**, 115020 (2016), [arXiv:1604.01776 \[hep-ph\]](#).
- [32] P. Asadi, M. Baumgart, P. J. Fitzpatrick, E. Krupczak, and T. R. Slatyer, *JCAP* **02**, 005, [arXiv:1610.07617 \[hep-ph\]](#).
- [33] K. Petraki, M. Postma, and J. de Vries, *JHEP* **04**, 077, [arXiv:1611.01394 \[hep-ph\]](#).
- [34] S. P. Liew and F. Luo, *JHEP* **02**, 091, [arXiv:1611.08133 \[hep-ph\]](#).
- [35] M. Garny, A. Ibarra, and S. Vogl, *Int. J. Mod. Phys. D* **24**, 1530019 (2015), [arXiv:1503.01500 \[hep-ph\]](#).
- [36] F. Giacchino, A. Ibarra, L. Lopez Honorez, M. H. G. Tytgat, and S. Wild, *JCAP* **02**, 002, [arXiv:1511.04452 \[hep-ph\]](#).
- [37] K. A. Mohan, D. Sengupta, T. M. P. Tait, B. Yan, and C. P. Yuan, *JHEP* **05**, 115, [Erratum: *JHEP* **05**, 232 (2023)], [arXiv:1903.05650 \[hep-ph\]](#).
- [38] C. Arina, B. Fuks, and L. Mantani, *Eur. Phys. J. C* **80**, 409 (2020), [arXiv:2001.05024 \[hep-ph\]](#).
- [39] C. Arina, B. Fuks, L. Mantani, H. Mies, L. Panizzi, and J. Salko, *Phys. Lett. B* **813**, 136038 (2021), [arXiv:2010.07559 \[hep-ph\]](#).
- [40] M. Becker, E. Copello, J. Harz, K. A. Mohan, and D. Sengupta, *JHEP* **08**, 145, [arXiv:2203.04326 \[hep-ph\]](#).
- [41] C. Arina, B. Fuks, J. Heisig, M. Krämer, L. Mantani, and L. Panizzi, *Phys. Rev. D* **108**, 115007 (2023), [arXiv:2307.10367 \[hep-ph\]](#).
- [42] C. Arina *et al.*, *Eur. Phys. J. C* **85**, 975 (2025), [Erratum: *Eur.Phys.J.C* **85**, 1105 (2025)], [arXiv:2504.10597 \[hep-ph\]](#).
- [43] S. Biondini, L. Tiberi, and O. Panella, *JHEP* **10**, 060, [arXiv:2507.00925 \[hep-ph\]](#).
- [44] P. Olgoso, P. Paradisi, and N. Selimovic, *The dark side of a tera-z factory* (2025), [arXiv:2507.17803 \[hep-ph\]](#).
- [45] B. D. Sáez, F. Rojas-Abatte, and A. R. Zerwekh, *Phys. Rev. D* **99**, 075026 (2019), [arXiv:1810.06375 \[hep-ph\]](#).
- [46] M. Becker, E. Copello, J. Harz, and M. Napetschnig, in preparation.
- [47] G. Belanger, F. Boudjema, A. Pukhov, and A. Semenov, *Nuovo Cim. C* **033N2**, 111 (2010), [arXiv:1005.4133 \[hep-ph\]](#).
- [48] S. Cassel, *J. Phys. G* **37**, 105009 (2010), [arXiv:0903.5307 \[hep-ph\]](#).
- [49] S. El Hedri, A. Kaminska, and M. de Vries, *Eur. Phys. J. C* **77**, 622 (2017), [arXiv:1612.02825 \[hep-ph\]](#).
- [50] T. Binder, A. Filimonova, K. Petraki, and G. White, *Phys. Lett. B* **833**, 137323 (2022), [arXiv:2112.00042 \[hep-ph\]](#).
- [51] M. Garny and J. Heisig, *Phys. Rev. D* **105**, 055004 (2022), [arXiv:2112.01499 \[hep-ph\]](#).
- [52] T. Binder, M. Garny, J. Heisig, S. Lederer, and K. Urban, *Phys. Rev. D* **108**, 095030 (2023), [arXiv:2308.01336 \[hep-ph\]](#).
- [53] M. Beneke, T. Binder, L. de Ros, M. Garny, and S. Lederer, *JHEP* **02**, 189, [arXiv:2411.08737 \[hep-ph\]](#).
- [54] N. D. Christensen, P. de Aquino, C. Degrande, C. Duhr, B. Fuks, M. Herquet, F. Maltoni, and S. Schumann, *Eur. Phys. J. C* **71**, 1541 (2011), [arXiv:0906.2474 \[hep-ph\]](#).
- [55] G. Alguero, G. Belanger, F. Boudjema, S. Chakraborti, A. Goudelis, S. Kraml, A. Mjallal, and A. Pukhov, *Comput. Phys. Commun.* **299**, 109133 (2024), [arXiv:2312.14894 \[hep-ph\]](#).
- [56] J. Harz and K. Petraki, *JHEP* **07**, 096, [arXiv:1805.01200 \[hep-ph\]](#).
- [57] P. O. Scherer and S. O. service), *Computational Physics*, 3rd ed., Graduate Texts in Physics, (Springer International Publishing :, Cham :, 2017.).
- [58] M. Garny, J. Heisig, B. Lülz, and S. Vogl, *Phys. Rev. D* **96**, 103521 (2017), [arXiv:1705.09292 \[hep-ph\]](#).
- [59] R. T. D'Agnolo, D. Pappadopulo, and J. T. Ruderman, *Phys. Rev. Lett.* **119**, 061102 (2017), [arXiv:1705.08450 \[hep-ph\]](#).